Barbaros Çetin[1]
S. Doğan Öner[1]
Besim Baranoğlu[2,3]

[1]Microfluidics & Lab-on-a-chip Research Group, Mechanical Engineering Department, Bilkent University, Ankara, Turkey
[2]Department of Manufacturing Engineering, Atılım University, Ankara, Turkey
[3]Computational Science and Engineering Laboratory, Atılım University, Ankara, Turkey

Received October 8, 2016
Revised January 21, 2017
Accepted January 21, 2017

Research Article

Modeling of dielectrophoretic particle motion: Point particle versus finite-sized particle

Dielectrophoresis (DEP) is a very popular technique for microfluidic bio-particle manipulation. For the design of a DEP-based microfluidic device, simulation of the particle trajectory within the microchannel network is crucial. There are basically two approaches: (i) point-particle approach and (ii) finite-sized particle approach. In this study, many aspects of both approaches are discussed for the simulation of direct current DEP, alternating current DEP, and traveling-wave DEP applications. Point-particle approach is implemented using Lagrangian tracking method, and finite-sized particle is implemented using boundary element method. The comparison of the point-particle approach and finite-sized particle approach is presented for different DEP applications. Moreover, the effect of particle–particle interaction is explored by simulating the motion of closely packed multiple particles for the same applications, and anomalous-DEP, which is a result of particle–wall interaction at the close vicinity of electrode surface, is illustrated.

Keywords:
Boundary element method / Dielectrophoresis / Lagrangian tracking method / Microfluidics
DOI 10.1002/elps.201600461

Additional supporting information may be found in the online version of this article at the publisher's web-site

1 Introduction

In microfluidic technology, manipulation of the bioparticles is the main ingredient for many of the diagnostic and clinical applications. Among several techniques available for the microfluidic manipulation of bioparticles, electrokinetic (EK) based methods such as electrophoresis and dielectrophoresis (DEP) are popular due to their favorable scaling with the reduced size of the system. DEP is the movement of a particle in a nonuniform electric field due to the interaction of the particle's dipole with the electric field gradient [1]. When the particle is placed in a nonuniform electric field, depending on the polarizibility of the particle and the medium, the particle may experience a net force in the direction of the electrical field gradient minima (negative-DEP, n-DEP) or maxima (positive-DEP, p-DEP). DEP has been studied extensively in the literature for particle manipulation in microfluidic systems mainly due to several advantages such as (i) its label-free nature, (ii) high selectivity, (iii) its favorable scaling effects, and (iv) the simplicity of the instrumentation [1].

DEP is applicable even for nonconducting particles and can be generated either by using direct current (DC) or alternating current (AC) field. In DC-DEP applications, electric field is applied by using external electrodes that are submerged into the reservoirs, and the flow is also induced by the electric field (i.e., electroosmotic flow). The nonuniform electric field is generated by means of the specially designed structures inside the microchannel network. In AC-DEP applications, an array of metal electrodes is placed inside the microchannel network. In the design of a DEP-based microfluidic system for the manipulation of particles, simulation (or numerical prototyping) is an important step in order to determine the most feasible and optimum geometry of the electrodes and the microchannel network. To assess

Correspondence: Dr. Barbaros Çetin, Microfluidics, and Lab-on-a-chip Research Group, Mechanical Engineering Department, Bilkent University, 06800 Ankara, Turkey
E-mail: barbaros.cetin@bilkent.edu, barbaroscetin@gmail.com
Fax: +90-312-266-4126

Abbreviations: **a-DEP**, anomalous dielectrophoresis; **AC-DEP**, alternating current dielectrophoresis; **BEM**, boundary element method; **CM**, Clausius–Mossotti factor; **DC-DEP**, direct current dielectrophoresis; **DEP**, dielectrophoresis/dielectrophoretic; **EK**, electrokinetic; **HST**, hydrodynamic stress tensor; **LTM**, Lagrangian tracking method; **MST**, Maxwell stress tensor; **n-DEP**, negative dielectrophoresis; **p-DEP**, positive dielectrophoresis; **PDMS**, polydimethylsiloxane; **tw-DEP**, traveling-wave DEP

Colour Online: See the article online to view Figs. 1–5 in colour.

the performance of the design, simulation of the particle trajectories is required. Since the trajectory of the particles is a result of interaction of particles with the fields, corresponding field variables need to be determined. For the DEP applications in microfluidics, the electrical potential field, flow field, and temperature field (if appreciable temperature gradients are present) have to be considered. To simulate the particle trajectories, there are two approaches.

(i) Point-particle approach: In this approach, the particles are treated as point particles, and Lagrangian tracking method (LTM) is implemented. The field variables solved without the presence of the particles, and the effect of the particle on the field variables is ignored, only the effect of the field variables on the particle is considered. Only the translational motion is taken into account and the rotational dynamics of the particles are ignored. To evaluate the particle trajectory, Newton's second law motion is applied for the particles. The external force on the particle is calculated by using prederived equations that calculate the drag force and DEP force. Therefore, these expressions needs to be know a priori. Typically, these kind of analytical expressions are known for some regular geometries such as spheres and ellipsoids; however, their derivations are usually based on a strong assumption that the particle is located in an infinite medium without any neighboring particle. Although there are some expressions to include effect of a single planar surface, a general expression that includes the confinement effect of a microchannel is not possible. Furthermore, point-particle approach does not include particle–particle interaction that can be quite important for creeping flow (strictly speaking, the volume fraction of the particles needs to be less than 1% to ignore the particle–particle interaction; [2], p. 576). Despite the ignorance of some these important effects, LTM has been applied for the simulation of particle motion in the literature for both DEP [3–8] and acoustophoretic applications [9, 10]. One major advantage of point-particle approach is that it does not require relatively high computational cost. Once the field variables are obtained without the presence of the particle, particle trajectories can be evaluated at the post-processing step. Therefore, LTM can be implemented for the motion of many particles that may allow statistical analysis [9, 10]. Researchers also proposed the use of an empirical correction factor that takes into account the particle–particle and particle–wall interaction. Using an empirical correction factor, a very good agreement has been observed with the experimental and numerical results [3–8]. This correction factor is between 0 and 1.0, depending on the size of the particle. If the particle size is small compared to the channel size, and the particle concentration is low enough (i.e., negligible particle–wall and particle–particle interactions), the correction factor becomes unity. If the particle size is large compared to the channel size and if the particle concentration is high, the correction factor tends to be different than zero. This correction factor depends on the channel geometry, flow rate, and the electric field; therefore, the prediction of this correction factor is based solely on experimental results.

(ii) Finite-sized particles: In this approach, the field variables are solved with the presence of the finite-sized particle, and the particle is moved as a result of this interaction. In each incremental movement of the particle, the field variables have to be resolved. The effect of the particle geometry, channel geometry, and particle–wall and particle–particle interactions can be captured. Once the field variables are obtained with the presence of finite particle size, the drag force on the particle can be determined by integrating the hydrodynamic stress tensor (HST), and an EK force can be determined by integrating the Maxwell stress tensor (MST). Furthermore, the torque induced on the particle can be obtained. This approach relaxes all the assumptions of LTM, and requires only the material properties of the medium and particle as a priori. However, since the HST and MST depend on the field variables' gradient on the particle surface, the field variables at the vicinity of the particle surface need to be obtained accurately. Since as the particles move within a microchannel, the mesh of the solution domain has to be deformed and/or remeshed. Therefore, from simulation point of view, these kind of simulations are challenging and computationally expensive. If numerical techniques based on domain mesh are implemented for these kind of problems, the meshing can be problematic to resolve the particle–particle and particle–wall interactions in a large domain and/or for many particles.

Although numerical techniques based on domain meshing such as finite element and finite volume have been implemented for simulations with finite-sized particles, to capture the physics of the particle–particle interaction and the movement of the particle within the domain different techniques have been implemented such as arbitrary Lagrangian-Eulerian method [11–14], immersed interface method/immersed boundary method [15–17], fictitious domain method [18, 19], sharp interface method [15–17] (the list of methods used for DEP modeling in the form of a table can be found elsewhere [17]). However, all those studies either include very few particles (one or two) or several particles in a relatively simple solution domain that does not resemble a microfluidic channel setting for DEP-based particle separation and/or sorting. Besides, the simulation settings include particles with relative large separation distance. At this point, boundary element method (BEM), which is a numerical technique based on boundary discretization, offers a unique advantage for simulations with finite-sized particles since it does not require remeshing. As the particle moves in the microchannel, the mesh elements on the particles translate and rotate. BEM is a very important numerical tool for the solution of the linear partial differential equations. Since the fluid flow inside the microchannels is governed by the Stoke's flow due to the low Reynolds number nature of

the flow, and electric field is governed by the Laplace equation, both field variables can be obtained using BEM. This unique feature of BEM has been exploited for the numerical design of electrical-mechanical traps for AC-DEP applications [20], the investigation of nonlinear EK particle–particle interactions [21], and the simulation of EK particle motion inside microchannels for DC-DEP applications [22, 23]. Recently, our group has developed a BEM-based solver for the simulation of particulate flow in microchannels [24–26]. In this study, we have extended our 2D solver to simulate DC-DEP, AC-DEP, and traveling-wave DEP (tw-DEP) applications. To verify our BEM solver, three benchmark problems are simulated, and our BEM solutions are compared with the experimental results and/or LTM results which is obtained using COMSOL Multiphysics. Moreover, the effect of particle–particle interaction has been explored by simulating the motion of nine closely-packed particles for DC-DEP, AC-DEP, and tw-DEP applications. The behavior of the particles at close vicinity of the electrode surface is a result of strong particle–wall interaction, which is named as anomalous DEP (a-DEP) [27], is also demonstrated. The unique contribution of this study is the comparison of the point-particle approach and finite-sized particle approach, and the demonstration of the particle–particle interaction for several DEP applications in microchannel settings that resemble DEP-based particle separation and/or sorting. In addition to these, this is the first time tw-DEP with finite-sized particle approach and a-DEP inside a microchannel setting that includes both the hydrodynamic and electric interaction of the particles with wall is demonstrated.

2 Theory

2.1 Governing equations

2.1.1 Point-particle approach

Assuming (i) constant thermophysical properties for the fluid and no thermal effect on flow field and particle velocity, (ii) the particle and the channel walls are nonporous and do not react with the surrounding liquid, (iii) the rotation of the particle does not affect the particle's translation motion, and (iv) the solution is dilute enough to neglect the electrostatic interaction between the particles, the particle position $\mathbf{x}_p$ can be determined, by integrating the particle velocity together with the initial position,

$$\mathbf{x}_p(t) = \mathbf{x}_o + \int_0^t \mathbf{u}_p(\tau)d\tau, \tag{1}$$

where $\mathbf{x}_o$ is the initial position of the particle, $\mathbf{u}_p$ is the particle velocity, and t is the time. For a fixed frame of reference, the translational motion of a particle under the action of hydrodynamic drag and DEP force can be written as

$$m_p \frac{d\mathbf{u}_p}{dt} = \mathbf{F}_H + \mathbf{F}_{EK}, \tag{2}$$

where m_p is the particle mass, $\mathbf{F}_H$ is the hydrodynamic drag force, and $\mathbf{F}_{EK}$ is the EK force (eletrophoretic and/or DEP) on the particle. The hydrodynamic drag force on a spherical particle is given by Stoke's law:

$$\mathbf{F}_{drag} = 6\pi\mu R(\mathbf{u} - \mathbf{u}_p), \tag{3}$$

at the creeping-flow limit, where R is the particle radius, $\mathbf{u}$ is the fluid velocity, and $\mathbf{u}_p$ is the particle velocity.

By using the phasor notation, time-averaged DEP force on a spherical particle in an AC-field (AC-DEP) can be expressed as [1]

$$\left\langle \mathbf{F}_{DEP}(t) \right\rangle = 2\pi\varepsilon_m \mathcal{R}e[f_{CM}] R^3 \nabla \mathbf{E}^2_{rms} + 4\pi\varepsilon_m Im[f_{CM}] R^3 \left(\mathbf{E}^2_{rms,i}\nabla\varphi_i\right), \tag{4}$$

where E_{rms} is the root-mean-square magnitude of the applied AC electric field, ε_m is the absolute permittivity of the suspending medium, and φ is the phase of the AC-field. Subscript i refers to each component of the electric field and the phase gradient. The last term in the parenthesis is a tensor notation and refers to the summation of the components of the vector quantities inside the bracket. f_{CM} is the Clausius–Mossotti (CM) factor, $\mathcal{R}e[\cdot]$ refers to the real part of CM and $Im[\cdot]$ refers to the imaginary part of CM. The first term depends on the nonuniformity in the electric field strength, and the second term depends on the nonuniformity in the phase of the electric field, which is the driving force for the twDEP applications. CM factor is given by

$$f_{CM}(\varepsilon_p, \sigma_p, \varepsilon_m, \sigma_m, \omega) = \frac{(\varepsilon_p - \varepsilon_m) + j/\omega(\sigma_p - \sigma_m)}{(\varepsilon_p + 2\varepsilon_m) + j/\omega(\sigma_p + 2\sigma_m)}, \tag{5}$$

where ε is the permittivity, σ is the electrical conductivity, and subscripts p and m stand for the particle and the medium, respectively. Note that when $\varepsilon_p > \varepsilon_m$, f_{CM} becomes positive, and when $\varepsilon_p < \varepsilon_m$, f_{CM} becomes negative. CM factor has numerical limits as -0.5 and 1.0. When DC-field is applied, the DEP force (DC-DEP) expressions remain the same; however, CM factor depends solely on electrical conductivities of the medium, and the frequency dependency of the CM disappears.

For the particle size considered in microfluidic applications, the characteristic time scale of acceleration is in the order of 10^{-4} s [3], which is much smaller than the time scale of the variation of the field variables. Therefore, the acceleration term can be safely neglected. Substituting Eqs. (4) and (3) into the Eq. (2), the particle velocity can be obtained as

$$\mathbf{u}_p = \mathbf{u} - \frac{\varepsilon_m R^2}{3\mu}\left[\mathcal{R}e\left[f_{CM}(\omega)\right]\nabla\mathbf{E}^2_{rms} + 2\ Im[f_{CM}]\left(\mathbf{E}^2_{rms,i}\nabla\varphi_i\right)\right]. \tag{6}$$

The trajectories of the particles can easily be obtained as a streamline plot, once the x- and y-component of the above equation are introduced as the x- and y-component of the stream function. As discussed earlier, this approach does not include the effect of any particle–wall and/or particle–particle interaction. Strictly speaking, this expression was derived based on the assumption that particles are embedded

in an infinite medium. To include effect of particle–particle and/or particle–wall interactions, an empirical correction factor can be introduced:

$$\mathbf{u}_p = \mathbf{u} - C\frac{\varepsilon_m R^2}{3\mu}\left[\mathcal{R}e\left[f_{CM}(\omega)\right]\nabla \mathbf{E}^2_{rms} + 2\ Im[f_{CM}]\left(\mathbf{E}^2_{rms,i}\nabla\varphi_i\right)\right]. \quad (7)$$

It is expected that for small particles, the correction factor approaches to unity, and for larger particles, it is between 0 and 1.0 depending on the size of the particle and microchannel, and needs to be determined experimentally. To be able to calculate the particle velocity, flow and electric field (i.e. **u**, **E**) have to be determined. However, the simplicity is that this field variables need to be obtained within the microchannel with the absence of any particles once by solving the Laplace, Navier–Stokes, and continuity equation with appropriate boundary conditions:

$$\nabla^2\hat{\phi} = 0, \quad (8)$$

$$\nabla\cdot\mathbf{u} = 0, \quad (9)$$

$$\rho(\mathbf{u}\cdot\nabla)\mathbf{u} = -\nabla p + \mu\nabla^2\mathbf{u}, \quad (10)$$

where ρ and μ are the density and the viscosity of the liquid medium, **u** is the flow field, p is the pressure field, $\hat{\phi}$ is the phasor of the electrical potential. These set of equations can be solved with any partial differential equations solver without any problem.

2.1.2 Finite-sized particle approach

In this approach, the flow and electric field need to be calculated together with the presence of the particle within the solution domain. Assuming rigid particle, the flow field is solved in the fluid domain; however, the electric field should be obtained both within the liquid domain and within the particle. The corresponding permittivity and conductivity values need to be assigned for both domains. Considering the low Reynolds number nature of the flow, Stokes equation can be solved to determine the flow field. Since the field variables are solved over and over again, such a simplification has a significant impact on the solution algorithm. The electric and flow fields can be obtained by solving the following equations with the appropriate boundary conditions:

$$\nabla\cdot\left[(\sigma + i\omega\varepsilon)\nabla\hat{\phi}\right] = 0, \quad (11)$$

$$\nabla\cdot\mathbf{u} = 0, \quad (12)$$

$$0 = -\nabla p + \mu\nabla^2\mathbf{u}. \quad (13)$$

Once the flow field and the electric field are determined, the hydrodynamic drag and EK force can be determined by integrating HST and MST (neglecting magnetic effects), which are given by

$$\mathbf{F}_H = \oint_S(\underline{\sigma}_H\cdot\mathbf{n})\,dS, \qquad \mathbf{F}_{EK} = \oint_S(\underline{\sigma}_{MST}\cdot\mathbf{n})\,dS. \quad (14)$$

Similarly, the hydrodynamic torque and EK torque can be determined by integrating moment on the particle due to HST and MST:

$$\mathbf{T}_H = \oint_S(\mathbf{x}-\mathbf{x}_p)\times(\underline{\sigma}_H\cdot\mathbf{n})\,dS,$$
$$\mathbf{T}_{EK} = \oint_S(\mathbf{x}-\mathbf{x}_p)\times(\underline{\sigma}_{MST}\cdot\mathbf{n})\,dS, \quad (15)$$

where $\mathbf{x}_p$ is the position of the center of the particle and **n** is unit vector normal to the surface. $\underline{\sigma}_h$ and $\underline{\sigma}_{MST}$ are defined as

$$\underline{\sigma}_H = -p\underline{\mathbf{U}} + \mu\left[\nabla\mathbf{u} + (\nabla\mathbf{u})^T\right],$$
$$\underline{\sigma}_{MST} = \varepsilon\left(\mathbf{E}\otimes\mathbf{E} - \frac{1}{2}\mathbf{E}^2\underline{\mathbf{U}}\right), \quad (16)$$

where $\underline{\mathbf{U}}$ is the unit tensor and symbol $\otimes$ denotes the dyadic product.

2.2 Boundary conditions

The boundary conditions applied in this study are summarized as follows:

- For DC-DEP applications, electric potential difference is applied at the channel inlet and exit. For the channel walls, electric insulation is assigned. For the flow field, pressure is equated to zero (if there exists a pressure driven flow on top of electroosmotic flow, pressure values can be assigned) at the channel inlet and exit. Using thin-double layer assumption, the slip velocity boundary condition is applied at the channel walls as

$$u_{slip,||} = -\frac{\varepsilon_m\zeta_w}{\mu}(\nabla\phi)_{||}, \quad (17)$$

  where ζ_w is the zeta potential of the channel wall. The same slip velocity is also defined on the particle surface by replacing the zeta potential with that of the particle.
- For AC-DEP simulations, electric potential is applied one electrode ($\hat{\phi}_o$) and zero potential is applied on the other electrode. All other boundaries assigned as insulated since the conductivity and emissitivity of the channel materials are low compared to the aqueous solution. For the flow field, since the solution domain is part of the larger microfluidic network, parabolic, fully-developed velocity profile with an average velocity of $U_{average}$ is applied at the inlet, pressure is equated zero at the exit, and no-slip boundary condition is applied on the channel walls.
- For tw-DEP applications, periodic boundary condition is applied for the electric field at the inlet and the exit, since the solution domain is the part of a reported microfluidic structure. Electric potential with a phase difference (φ) is assigned on the electrode surfaces. For the remaining boundaries, insulated boundary condition is applied. Considering the frequency and the conductivity of the medium [1], no-slip boundary condition is applied both

on the electrodes and the channel walls. Parabolic velocity profile with an average velocity of $U_{average}$ is applied at the inlet, pressure is equated zero at the exit.

3 Boundary element formulation

Modeling of DEP motion of with BEM requires two explicit steps: (i) solution of the electric field equation that presents the EK forces to the particle(s) and (ii) solution of the Stokes flow equation that determines the velocity of the particle that can be integrated to obtain the particle trajectory. The boundary element equation for electric field equation (i.e., Laplace Equation) can be written as

$$C(A)\phi(A) + \int_S q^*(A,\ P)\hat{\phi}(P)\mathrm{d}S = \int_S \phi^*(A,\ P)\hat{q}(P)\mathrm{d}S, \quad (18)$$

where A is the source point and P is the field point. In Eq. (18), $\hat{\phi}$ represents the phasor of the electric potential, and $\hat{q}$ represents the corresponding normal flux on the boundary. The first and second fundamental solutions of the Laplace equation are represented by ϕ^* and q^*, respectively, and the constant $C(A)$ takes values depending on the position of the source point A: If A is inside the solution domain, $C(A) = 1$, if A is on a smooth boundary $C(A) = 1/2$, if A is outside the solution domain $C(A) = 0$. In this study, only constant elements are employed, which means all nodes are on smooth boundary. When the boundary of the solution domain is discretized using N constant elements, the integral equation becomes

$$\mathbf{H}^{\phi} \cdot \boldsymbol{\phi} = \mathbf{G}^{\mathrm{u}} \cdot \mathbf{q}. \quad (19)$$

Here, $\boldsymbol{\phi}$ represents the column vector that is composed of the boundary quantities (at the boundary nodes) of the phasor of the electric potential, $\mathbf{q}$ represents the corresponding fluxes at the boundary nodes and $\mathbf{H}^{\phi}$ and $\mathbf{G}^{\phi}$ are the system matrices constructed using the fundamental solutions of the Laplace equation. Note that for AC-DEP and tw-DEP applications, the components of these matrices and vectors are complex valued. The number of equations in this system of equations is equal to the number of nodes on the boundary; and since in this study, constant elements are employed, it is equal to the number of elements that are used to discretize the boundaries of the solution domain. The total number of unknowns presented with Eq. (19) is $2N$, where N is the number of nodes on the boundaries. Through the imposition of proper boundary conditions, N of these quantities are pre-determined leading to a solvable system of linear equations. The solution of the equations lead to the determination of the phasor of the electric potential ($\hat{\phi}$) at each boundary node along with the normal flux. For the evaluation of the MST that leads to the $\mathbf{F}_{EK}$, the proper determination of $\mathbf{E}$ ($= -\nabla\hat{\phi}$) is required. The solution, on the other hand, gives only the normal flux. Thus, the tangential variation of $\hat{\phi}$ has to be evaluated for tangential components of $\mathbf{E}$. Finite difference scheme with central differencing is employed within the nodal values of $\hat{\phi}$ for the determination of the tangential component.

A well-established literature stands for the solution of Stokes equation using BEM [24]. The boundary element equation for Stokes equations can be written as

$$C_{ij}(A)u_j(A) + \int_S t^*_{ij}(A,\ P)u_i(P)\mathrm{d}S = \int_S u^*_{ij}(A,\ P)t_i(P)\mathrm{d}S, \quad (20)$$

where u_i are the components of the velocity vector and t_i are the components of the traction vector at the given point. The first and second fundamental solutions of Stokes equation are represented by u^*_{ij} and t^*_{ij}, respectively. Constants $C_{ij}(A)$ take values depending on the position of the point A: If A is inside the solution domain, $C_{ij}(A) = \delta_{ij}$; if A is on a smooth boundary $C_{ij}(A) = \delta_{ij}/2$; and if A is outside the solution domain $C_{ij}(A) = 0$. The resulting system of equations are very similar to those of Eq. (19):

$$\mathbf{H}^{\mathrm{u}} \cdot \mathbf{u} = \mathbf{G}^{\mathrm{u}} \cdot \mathbf{t}, \quad (21)$$

where $\mathbf{u}$ is a vector that involves the components of the velocity field vector at each boundary node (which would be 2×2 vectors for each node) and $\mathbf{t}$ is a vector that involves the components of the corresponding traction vector at the same boundary nodes. The system matrices, $\mathbf{H}^{\mathrm{u}}$ and $\mathbf{G}^{\mathrm{u}}$ are $2N \times 2N$ matrices constructed using the fundamental solutions of the Stokes equation. The system of equations presented in matrix for in Eq. (21) contains $2N + 2N = 4N$ unknowns, $2N$ of which is expected to be determined through the boundary conditions imposed on the system. It is a common practice to impose either the component of the velocity or the component of the traction or a combination in a given direction at each node as boundary condition. But, in case of particle flow, neither of these three is explicitly known. Thus, the imposition of the boundary conditions requires the physical insight to the kinetics of the flowing particle. At this point, it is assumed that the particles are buoyant, thus the only external force imposed on the particle(s) would be $\mathbf{F}_{EK}$ other than hydrodynamic interaction. Furthermore, assuming rigid particles, the motion characteristic is 2D rigid-body motion, which means each boundary point has a velocity given by

$$u_i = u^b_i + \omega r \hat{t}_i, \quad (22)$$

u_i are the components of the velocity vector at a node on the boundary of the particle (with i representing the direction), u^b_i are the components of the velocity vector at the selected center of the rigid particle, ω is the angular velocity of the particle, r is the distance between the selected center and the boundary node, and $\hat{t}$ are the components of the unit-perpendicular vector to the vector drawn from the center to the node. The imposition of this rigid-body motion (the summation of the forces and the moments are equal to zero) condition is discussed in detail in [24], where the matrix $\mathbf{H}^{\mathrm{u}}$ should be augmented with three columns per particle—the components of the first column are evaluated by summing up the corresponding components of the odd columns, the components of the second column are evaluated by summing up the corresponding components of the even columns, and the third column is evaluated by summing up the corresponding

components of the odd columns after multiplication with $r\hat{t}_1$ and the even columns after multiplication with $r\hat{t}_2$. After augmenting the matrix $\mathbf{H}^u$ with three columns, for the system of equations to be solvable, three additional equations should be imposed. These three equations are obtained using the static equilibrium equations that lead to the determination of the translational velocity of the particle's center and the angular velocity of the particle. Once the translational and angular velocity of the particle is obtained, the trajectory and the rotation of the particle is achieved through time integration. The fundamental solutions for Laplace and Stokes equation can be found in BEM literature [28].

4 Results and discussion

In BEM analysis, unless otherwise stated, one boundary element per micrometer is used for discretizing the channel walls, and two boundary elements per micrometer is used for discretizing the particle boundary. Constant elements are implemented. Euler's method is implemented for time integration. The convergence of the particle trajectory is achieved by the time step of $dt = 0.001$ s for all the simulations. The convergence criteria are set as the deviation of the final position of the particle is less than the 10% of the particle diameter, which is well-below the uncertainty limit of a measurement of a particle's location in an experiment. Numerical integrations are performed using Gauss-quadrature with 24 points. Singular integrals are evaluated analytically. All the dimensions given in the figures are in μm unless otherwise is stated.

4.1 Benchmark solutions

The boundary element formulation developed has been tested for three different benchmark problems that are for DC-DEP, AC-DEP, and tw-DEP applications. For the LTM results, the flow and electric field is simulated without the presence of the particles as described in Section 2.1, and at the postprocessing step the particle trajectories are generated. For the simulation of the flow and electric field, COMSOL multiphysics simulation environment is implemented.

For the DC-DEP application, the experimental results of Kang et al. [3] is used where the experiments were conducted with a dilute solution in terms of particle concentration (particle concentration was reported as 10^5 particles/mL, and the flow rate is estimated as 0.12 μL/min). First, all the results are digitized. A total of 5.7 and 15.7 μm particles are released from different y-locations, for different electric field values as seen in Fig. 1. The simulation parameters are as follows: $\sigma_m = 10^{-3}$ S/m, $\sigma_p = 10^{-6}$ S/m, $\zeta_w = -80$ mV, $\zeta_p = -32$ mV, and $\varepsilon_m = 80\varepsilon_o$. The y-locations are normalized with respect to the width of the channel. The solid lines show the LTM results with an empirical constant. This empirical constant was taken from the reported results. As seen from the results, BEM can predict the particle trajectories without any need for an empirical constant at this dilute limit where the particle–particle interaction does not play an essential role. Furthermore, the final position of the particles for each electric field is obtained in a good agreement with the experimental results. For the larger particles and for the initial y-locations close to the lower and upper walls, BEM results predict the final position of the particle better than the LTM results. This effect is more pronounced for the case of lower electric field strength. Actually, for this application, the particle–wall interaction is a key parameter, which was taken care of with a separate term in LTM formula in [3]. BEM does not need any addition information to resolve this interaction.

For the AC-DEP application, the experimental results of Cetin and Li [7], which demonstrated the size-based DEP separation of latex particles, are used. Again, the experiments were conducted at the dilute limit (particle concentration was reported as 10^5 particles/mL, and the flow rate is estimated as 0.08 μL/min). Since the volumetric flow rate was not specified, the velocity of 5 and 10 μm particles is obtained from the digitized data. Then, the flow field is adjusted to match the velocity of the particles for the initial time steps. The experimental results together with BEM and LTM results are presented in Fig. 2. The LTM results are generated with the empirical constants reported in [7]. The simulation parameters are as follows: $\varepsilon_m = 80\varepsilon_o$, $\varepsilon_p = 2.5\varepsilon_o$, $\sigma_m = 10^{-4}$ S/m, $\sigma_p = 8 \times 10^{-4}$ S/m (for 5 μm particles), $\sigma_p = 4 \times 10^{-4}$ S/m (for 10 μm particles), $\hat{\phi}_o = 10$ V, $f = 500$ kHz. It can be clearly seen that BEM can capture motion of both particles successfully. The n-DEP behavior of the particles also mimicked without assigning any value for the CM factor. The force predicted as a result of the integration of the MST. Again, without any need for predescribed empirical constant, BEM can predict the particle trajectories at the dilute limit.

For the tw-DEP application, the benchmark problem generated using the geometry reported in [29]. For the comparison, LTM is also implemented. The simulation parameters are the following: $\varepsilon_m = 80\varepsilon_o$, $\varepsilon_p = 2.5\varepsilon_o$, $\sigma_m = 10^{-4}$ S/m, $\sigma_p = 8 \times 10^{-4}$ S/m (for 5 μm particles), $\sigma_p = 4 \times 10^{-4}$ S/m (for 10 μm particles), $\hat{\phi}_o = 10$ V, $f = 1$ MHz (for n-DEP), $f = 100$ kHz (for p-DEP). The correction factor is determined to match the BEM results, and the results are turned out to be as expected. The correction factor is close to unity for the smaller particles. It can clearly be seen from Figure 3, the correction factor is function of the flow velocity, too. As the flow velocity increases, the velocity gradients increase within the flow field which means a larger disturbance with the presence of the particles. It is clear that tuning the correction factor, the actual trajectories can be predicted.

One important conclusion regarding these benchmark simulations is that BEM can predict the particle trajectory without any correction factor at the dilute particle concentration limit. Furthermore, BEM can also predict the rotational motion of the particles, which is neglected for the point-particle approach (please see Supporting Information Video S1 and Video S2). BEM can also predict the empirical correction factor without any need for actual experiments. For a given particle size and flow conditions, a correction factor can be predicted based on BEM simulations of a

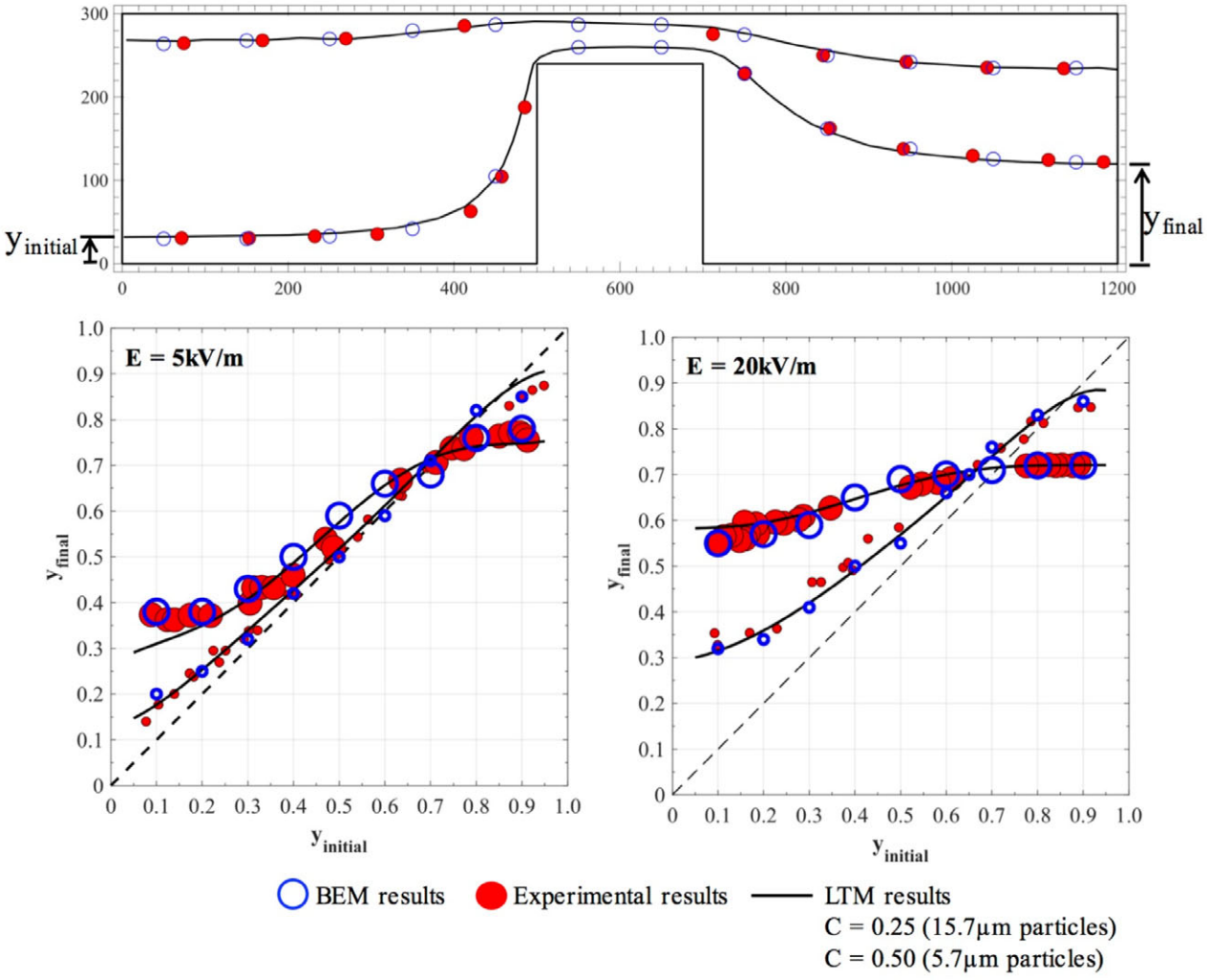

Figure 1. Comparison of BEM results with experiments and LTM (DC-DEP).

single particle for each particle may be at a relative small domain. Then, the particle trajectory of particles released from different locations for a larger domain can be generated by using point-particle approach that would allow researchers to have realistic particle trajectory predictions at the design step without any extensive computational cost. Moreover, BEM supported LTM simulations can be performed to analyze the effect of any size and/or release point variation.

4.2 Multiparticle simulations

In the design of the DEP-based microfluidic devices, typically point-particle approach is utilized that ignores particle–particle interactions. However, the experiments are usually conducted with relative large particle concentrations, which makes the neglection of particle–particle interaction questionable. In this section, a new numerical setting is prepared to demonstrate the effect of the particle–particle interactions on the particle trajectory for all three applications. All the simulation parameters are kept the case, only the number of particles inside the microchannel is increased to discuss the effect of multiparticles. Nine 15 μm particles with a particle spacing of $d_p = 15\,\mu m$ are released from different y–locations. The geometric parameters are given in the caption of the figure. To compare, single particles are also released from the same y-locations. The result of the single-particle simulations are given with the solid lines. The schematic drawing of the set-up problems together with the normalized y-locations for the initial and final states are plotted in Fig. 4.

The results for DC-DEP application is presented in Fig. 4A. As seen from the figure, when multiparticles are released at the same time, the final y-locations of the particles are quite different than that of the single-particle, which is due to the distortion of the electric and flow field with the presence of the other particles at the vicinity of a particle. This final y-location is very important when the manipulation of the particles is concerned. The video of this simulation can be found in the Supporting Information Video S1). Moreover, it can be observed in the video that the effect of the

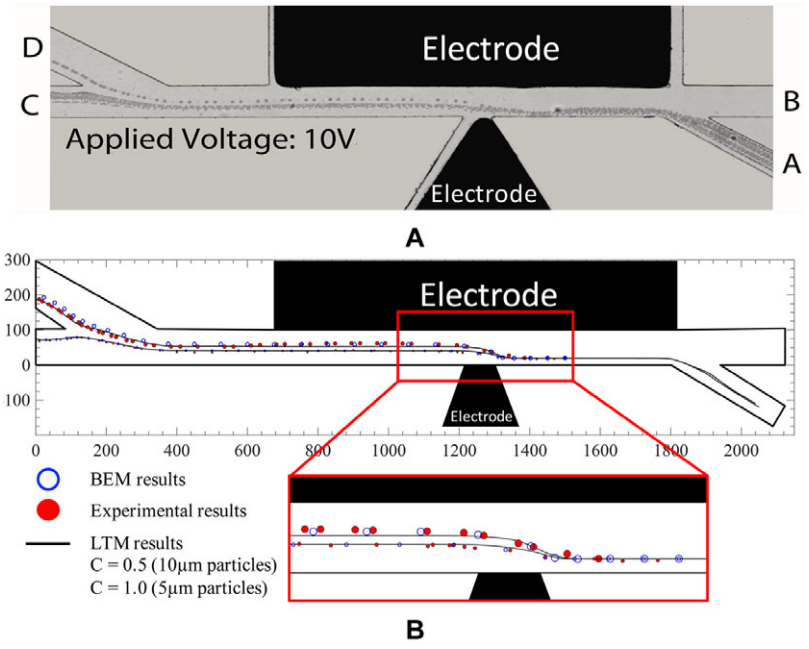

Figure 2. Comparison of BEM results with experiments and LTM (AC-DEP): **(A)** experimental, **(B)** comparison.

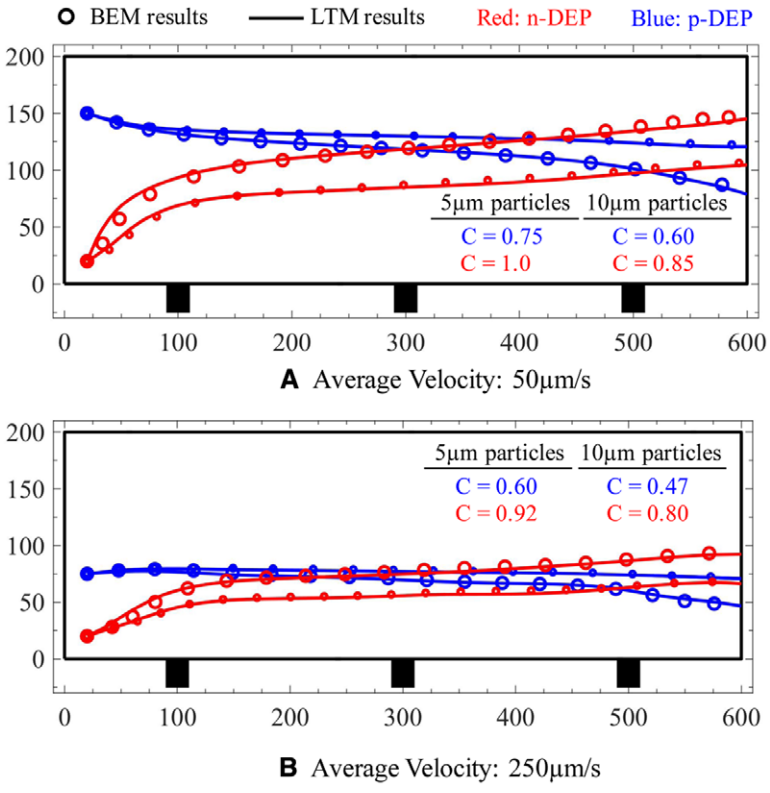

Figure 3. Comparison of BEM results with LTM (tw-DEP).

rotation of the particles is quite important and affected by the particle–particle interactions. At this point, it should be noted that the thin-double layer assumption is questionable for the particles with very small particle separation; therefore, the actual particle dynamics may also be different especially when the particles pass the hurdle structure. But, one important conclusion based on this simulation is that LTM cannot predict the actual picture for the multiple particles since group of particles have a significant disturbance on the flow and electrical field together with complex particle–particle interactions. The disturbance induced by the multiple particles on the electric and flow fields is more severe than that of a

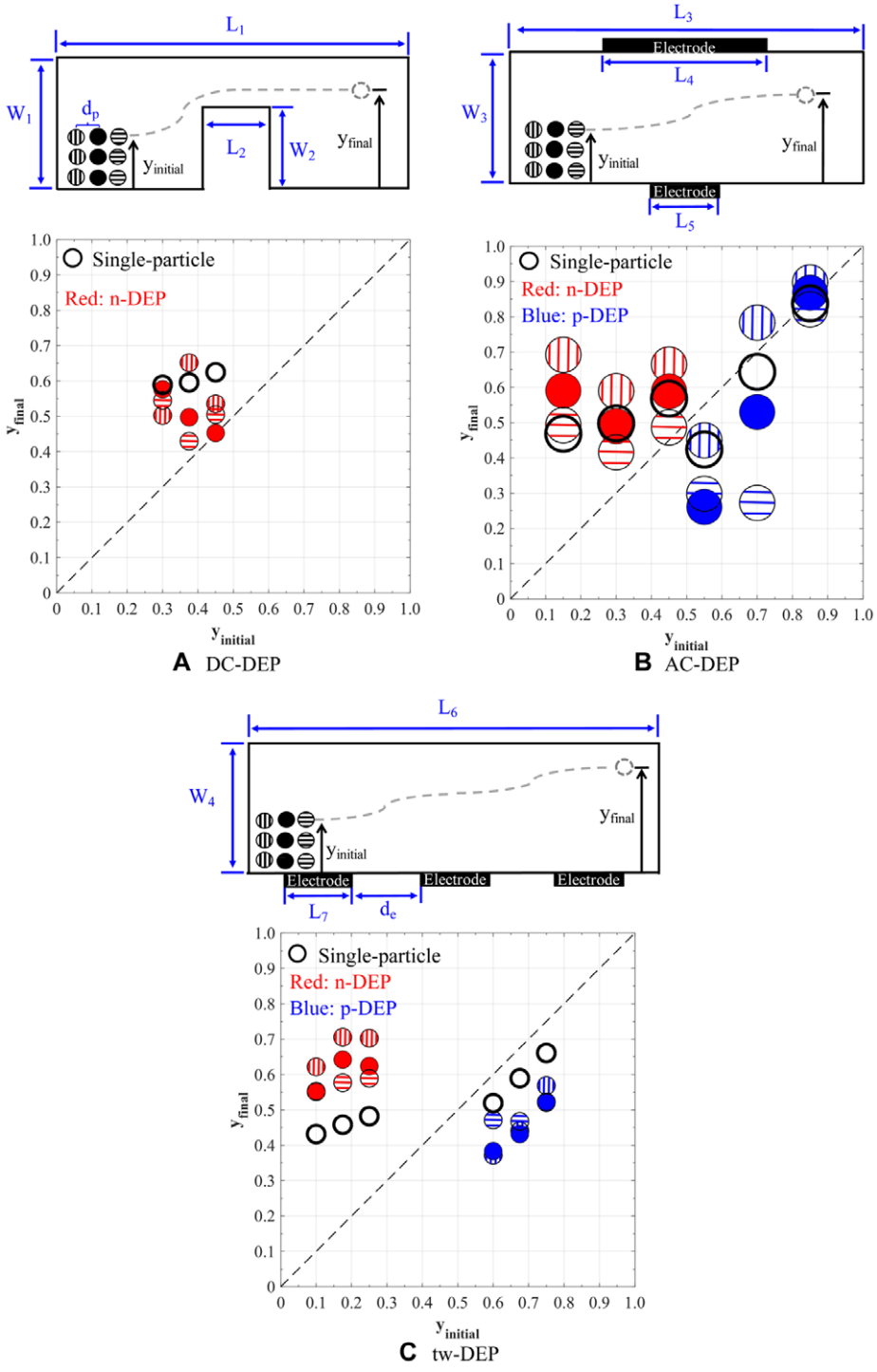

Figure 4. Effect of particle–particle interaction: (A) DC-DEP, (B) AC-DEP, (C) tw-DEP.

single particle. Besides, presence of multiple particles includes also particle–particle interaction, which additionally affects the particle trajectories in the microchannel.

The results for AC-DEP application are illustrated in Fig. 4B. Both n-DEP and p-DEP particles are released. n-DEP particles are released from the locations closer to the lower wall, and the p-DEP particles are released from the locations closer to the upper wall (since the trajectory of a n-DEP particle moving closer to the upper wall is not interesting, so is the p-DEP particle moving closer to the lower wall). It can be observed that the particle–particle interaction may affect the final location of the particles quite significantly, again. This variation can significantly alter the performance of a microfluidic device designed for particle separation or sorting. The video of this simulation can be found in Supporting Information Video S2). It can be observed in the

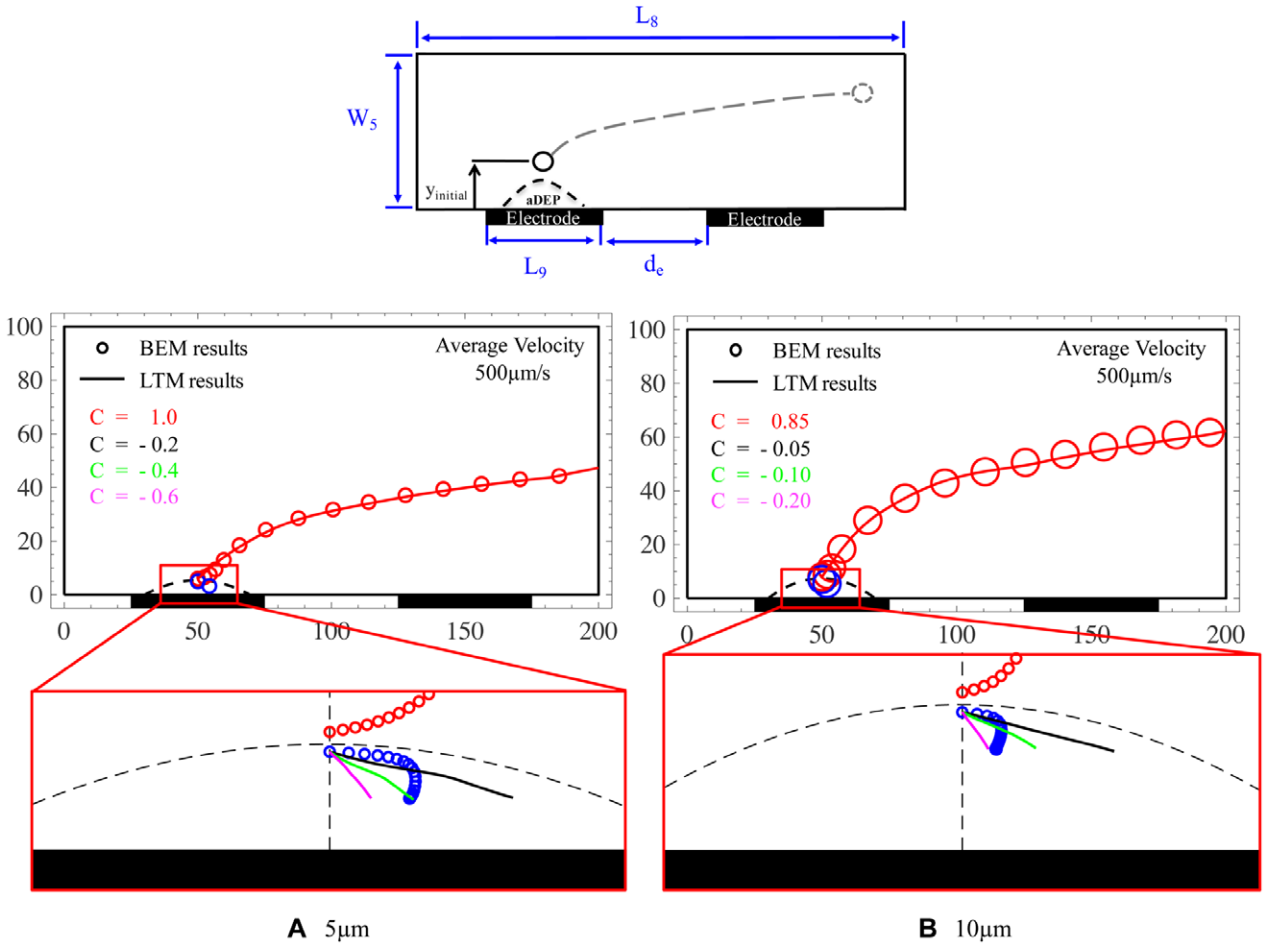

Figure 5. Effect of particle-wall interaction (a-DEP): (A) 5 μm, (B) 10 μm ($W_5 = 100\,\mu m$, $L_8 = 200\,\mu m$, $L_9 = 50\,\mu m$, $d_e = 50\,\mu m$).

video the particles at the same y–locations tend to create a chain that enhances the DEP force since chained particles tend to behave like a particle with a larger size for the n-DEP case. However, for the p-DEP case, the particles tend to create a chain of two particles that enhances the DEP force, again. The chained particles have totally different translational and rotational dynamics.

The results for tw-DEP application are illustrated in Fig. 4C. n-DEP particles are released from the locations closer to the lower wall, and the p-DEP particles are released from the locations closer to the upper wall. Likewise in AC-DEP application, the deviation of the multiparticle behavior is significantly different than that of single-particle, since the particles at the same y-locations tend to create a chain of three particles that enhances the DEP force for n-DEP case (please see Supporting Information Video S3). For p-DEP case, although there is no chain formation, the particles dynamics are quite different than that of single particle due to the strong particle–particle interactions.

The MST formulation is valid for particles with any arbitrary geometry. Therefore, as a final simulation, the motion of fifteen particles with different size and geometry is simulated for an AC-DEP application. Different conductivity values are assigned for the particles. The results of the simulation can be seen in Supporting Information Video S4. The particle trajectories are obtained without defining any empirical constant and any CM factor value. The motion is solely result of the interaction of the particles with the electric and flow fields. The prediction of the CM factor for geometries other than sphere also needs some special care. The CM factor needs to be predicted based on the expression valid for a given shape. In the case of BEM, the response is calculated based on the stress induced on the particle surface, as long as the MST calculated on the particle surface, the response of the particle can be predicted with the solely based on the physics of the problem. It should also be noted that when the particles form a chain-like structures, the CM factor of this structure is also different than the CM factor of the isolated particles.

4.3 Anomalous DEP (a-DEP) simulations

The DEP force acting on a particle given by Eq. (4) is valid for the particles embedded in an infinite medium. For the cases where there is strong particle-wall interaction (i.e., particle moving at the close vicinity of the channel wall), the

motion of the particle cannot be modeled with this expression. Recently, Camarda et al. [27] defined a region at the close vicinity of the electrode and defined the phenomena as a-DEP. To demonstrate the a-DEP in a micro-channel setting with flow, a simulation setup is generated for 5 and 10 μm particles. The schematic drawing of the simulation setup is given in Fig. 5. The simulation parameters are the following: $\varepsilon_m = 80\varepsilon_o$, $\varepsilon_p = 2.5\varepsilon_o$, $\sigma_m = 10^{-4}$ S/m, $\sigma_p = 8 \times 10^{-4}$ S/m (for 5 μm particles), $\sigma_p = 4 \times 10^{-4}$ S/m (for 10 μm particles), $\hat{\phi}_o = 10$ V, $f = 1$ MHz. Since the particles may be very close to the wall, the boundary element size is dropped to four elements per micrometer, and the time step is dropped to 10^{-4} s, and the same convergence criteria is set. The particles with negative CM factor (i.e., n-DEP) are released from different height locations. The results are shown in Fig. 5, a-DEP region is also indicated with dashed line on the figure. Only the results for two particles are demonstrated in the figure for clarity of the figure. As predicted by Camarda et al. [27], the particles released from outside the a-DEP region, behaves like a n-DEP particle and pushed by the electrode, and the particles released within a-DEP region, regardless of their CM factor, they are attracted by the electrode and reach an equilibrium position at the vicinity of the electrode. The results of the LTM are also included. For the particles released outside the a-DEP region, LTM can predict the particle motion; however, careful inspection reveals that at the close vicinity of the a-DEP region, there exists some deviation between LTM and BEM that does not effect the final position of the particles. The situation is more complex for the particle released within the a-DEP region. Several LTM results are also included. It is clear that LTM needs a negative coefficient to predict the behavior, however simple correction factor cannot predict the particle motion. Since the particle-wall interaction is very dominant, a simple correction factor cannot include the effect of the particle–wall interaction. The particles are attracted by the electrode surface and then they reach an equilibrium position that is approximately 200 nm away from the wall, and particles no longer have translational motion but only a rotational motion (see Supporting Information Video S5). This equilibrium position is the result of strong hydrodynamic and electrical interaction between the particle and the wall. As long as small enough elements and small enough time step are used, BEM can model these interactions physically without any need for additional contact models.

5 Concluding remarks

In this study, we discussed the modeling of DEP particle motion in a micro-channel. Point-particle approach is implemented by LTM, and finite-sized particle is implemented by BEM. Formulations are discussed for DC-DEP, AC-DEP, and tw-DEP applications. It is observed that BEM results can predict the particle trajectories without any need for any tuning parameter. Moreover, BEM can also predict the value of the tuning parameter without any need for experimental data. In the BEM analysis, it is also observed that single-particle behavior is quite different than that of the multiparticle behavior. The disturbance induced by the multiple particles on the electric and flow fields is more severe than that of a single particle. Besides, presence of multiple particles includes also particle–particle interaction, which additionally affects the particle trajectories in the microchannel. One of the significant conclusion of this study is that the LTM method without/with correction factor is valid at the dilute limit of the particle concentration. As many particles are introduced in the domain, the particle–particle interactions dominate the particle motion, and the resulting trajectories well beyond the capabilities of the LTM.

The particle–wall interaction is also demonstrated for a-DEP case. Without any need for hydrodynamic and electric field interaction, BEM can predict the a-DEP behavior. The particles released within a-DEP region are found to be trapped at the vicinity of the electrode surface, and the particles released from the outside of the a-DEP region are found to behave like a regular particle. The behavior of the multiparticles in a-DEP has not been explored; however, we believe that very interesting particle behavior can be observed when the hydrodynamic and electric interaction couples. The investigation of behavior of multiparticles in a-DEP region will be one of our future research directions.

The behavior of high-concentration suspensions flowing through micro-channels in the presence of external forces is a challenging problem. For such a case, the monitor of behavior of each particle is a quite challenging and requires a very high computational cost. The computational cost can be reduced significantly by continuum modeling based on effective-medium theory [30, 31]. The key parameter for such models is the effective transport properties as a function of particle concentration such as density, viscosity, and DEP mobility. These parameters can be determined in a simulation setup for a certain region of the microchannel, and the extended picture can be obtained with the continuum model for the entire system. Once we extent our study to 3D, the transport properties of a particle suspension with different particle concentration can be predicted for continuum type modeling. Furthermore, different physical phenomena other than DEP such as acoustophoresis and thermophoresis may also be included

BEM has a very favorable parallelization nature that can significantly speed up the simulations especially for 3D problems. Therefore, CPU/GPU parallelization of our BEM formulation will also be studied in the near future. We would like to also focus our attention for the preparation of an experimental setup for the verification of the multiparticle cases.

The authors have declared no conflict of interest.

6 References

[1] Cetin, B., Li, D., *Electrophoresis* 2011, *32*, 2410–2427.

[2] Leal, L. G., *Advanced Transport Phenomena: Fluid Mechanics and Convective Transport Processes*, Artech House, Cambridge, UK, 2006, pp. 164–168.

[3] Kang, K. H., Xuan, X., Kang, Y., Li, D., *J. Appl. Phys*. 2006, *99*, 1–8.

[4] Kang, Y., Cetin, B., Wu, Z., Li, D., *Electrochim. Acta* 2009, *54*, 1715–1720.

[5] Cetin, B., Kang, Y., Wu, Z., Li, D., *Electrophoresis* 2009, *30*, 766–772.

[6] Cetin, B., Li, D., *Electrophoresis* 2009, *30*, 3124–3133.

[7] Cetin, B., Li, D., *Electrophoresis* 2010, *31*, 3035–3043.

[8] Zeinali, S., Cetin, B., Oliaei, S., Karpat, Y., *Electrophoresis* 2015, *36*, 1432–1442.

[9] Cetin, B., Buyukkocak, S., Zeinali, S., Ozer, B., *ASME 4th International Conference on Micro/Nanoscale Heat and Mass Transfer*, No. 22181, 11–14 December 2013.

[10] Buyukkocak, S., Ozer, M. B., Cetin, B., *Microfluid. Nanofluid*. 2014, *17*, 1025–1037.

[11] Ai, Y., Joo, S. W., Jiang, Y., Xuan, X., Qian, S., *Electrophoresis* 2009, *30*, 2499–2506.

[12] Ai, Y., Beskok, A., Gauthier, D. T., Joo, S. W., Qian, S., *Biomicrofluidics* 2009, *3*, 044110.

[13] Ai, Y., Qian, S., *J. Colloid Interface Sci*. 2010, *346*, 448–454.

[14] Ai, Y., Zeng, Z., Qian, S., *J. Colloid Interface Sci*., 2014, *417*, 72–79.

[15] Kang, S., *Comput. Fluids* 2013, *73*, 10–23.

[16] Kang, S., *Comput. Fluids* 2014, *105*, 231–243.

[17] Kang, S., *Eur. J. Mech. B Fluids* 2015, *54*, 53–68.

[18] Shi, Y., Yu, Z., Shao, X., *Particuology* 2010, *8*, 351–359.

[19] Shi, Y., Yu, Z., Shao, X., *Powder Technol*. 2011, *210*, 52–59.

[20] Le, D. V., Rosales, C., Khoo, B. C., Perairea, J., *Lab Chip* 2008, *8*, 755–763.

[21] Saintillan, D., *Phys. Fluids* 2008, *20*, 067104.

[22] House, D. L., Luo, H., *Eng. Anal. Bound. Elem*. 2010, *34*, 471–476.

[23] House, D., Luo, H., Chang, S., *J. Colloid Interface Sci*. 2012, *374*, 141–149.

[24] Cetin, B., Baranoglu, B., in: Li, D. (Ed.), *Encyclopedia of Microfluidics and Nanofluidics*, 2nd edition, Springer, Boston, MA, 2015, pp. 202–213.

[25] Karakaya, Z., Baranoglu, B., Cetin, B., Yazici, A., *Comp. Model. Eng. Sci*. 2015, *104*, 227–249.

[26] Solmaz, M. E., Cetin, B., Baranoglu, B., Serhathoglu, M., Biyikli, N., *Proceedings of SPIE*, Vol. 9548, 2015, 95481D–95481D–8.

[27] Camarda, M., Scalese, S., Magna, A. L., *Electrophoresis* 2015, *36*, 1396–1404.

[28] Wrobel, L. C., *Boundary Element Method Volume 1: Applications in Thermo-Fluids and Acoustics*, Wiley, West Sussex 2002.

[29] Liu, D., Garimella, S. V., *Nanosc. Microsc. Therm*. 2009, *13*, 109–133.

[30] Nicotra, O., Magna, A. L., Coffa, S., *J. Appl. Phys*. 2009, *95*, 073702.

[31] Ley, M. W. H., Bruus, H., *Lab Chip* 2016, *16*, 1178–1188.

